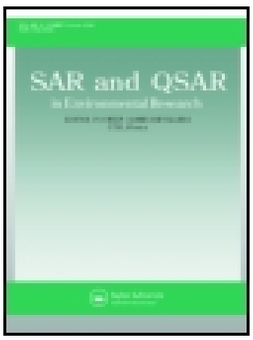

SAR and QSAR in Environmental Research

ISSN: (Print) (Online) Journal homepage: https://www.tandfonline.com/loi/gsar20

9-Arylimino noscapinoids as potent tubulin binding anticancer agent: chemical synthesis and cellular evaluation against breast tumour cells

A.K. Patel, R.K. Meher, P.K. Nagireddy, P. Pragyandipta, R.K. Pedapati, S. Kantevari & P.K. Naik

To cite this article: A.K. Patel, R.K. Meher, P.K. Nagireddy, P. Pragyandipta, R.K. Pedapati, S. Kantevari & P.K. Naik (2021): 9-Arylimino noscapinoids as potent tubulin binding anticancer agent: chemical synthesis and cellular evaluation against breast tumour cells, SAR and QSAR in Environmental Research, DOI: 10.1080/1062936X.2021.1891567

To link to this article: https://doi.org/10.1080/1062936X.2021.1891567

SAR AND QSAR IN ENVIRONMENTAL RESEARCH
https://doi.org/10.1080/1062936X.2021.1891567

Taylor & Francis
Taylor & Francis Group

9-Arylimino noscapinoids as potent tubulin binding anticancer agent: chemical synthesis and cellular evaluation against breast tumour cells

A.K. Patel[a], R.K. Meher[a], P.K. Nagireddy[b], P. Pragyandipta[a], R.K. Pedapati[b], S. Kantevari[b], and P.K. Naik[a]*

[a]Centre of Excellence in Natural Products and Therapeutics, Department of Biotechnology and Bioinformatics, Sambalpur University, Burla, Sambalpur, India; [b]Fluoro and Agrochemicals Division, CSIR-Indian Institute of Chemical Technology, Hyderabad, India

ABSTRACT

A library of 9-arylimino derivatives of noscapine was developed by coupling of Schiff base containing imine groups. Virtual screening using molecular docking with tubulin revealed three molecules, 12–14 that bind with high affinity. An improved predicted free energy of binding (FEB) of −5.390, −6.506 and −6.679 kcal/mol for the molecules 12–14 was found compared to noscapine (−5.135 kcal/mol). Furthermore, molecular dynamics simulation in combination with Molecular Mechanics Poisson-Boltzmann Surface Area (MM-PBSA) revealed robust binding free energy of −166.03, −169.75 and −170.63 kcal/mol for the molecules 12, 13 and 14, respectively. These derivatives were strategically synthesized and experimentally validated for their anticancer activity. Tubulin binding assay revealed substantial binding of molecules 12–14 with purified tubulin. Further, their anticancer activity was demonstrated using two cancer cell lines (MCF-7 and MDAMB-231) and a panel of primary breast tumour cells. All these derivatives inhibited cellular proliferation in all the cancer cells that ranged between 30.1 and 5.8 μM, which is 1.7 to 7.52 fold lower than that of noscapine. Further, these novel derivatives arrest cell cycle in the G2/M-phase followed by induction of apoptosis. Thus, 9-arylimino noscapinoids 12–14 have a great potential to be a novel therapeutic agent for breast cancers.

ARTICLE HISTORY
Received 12 November 2020
Accepted 14 February 2021

KEYWORDS
Noscapine; 9-arylimino noscapinoids; tubulin binding; anticancer agents; breast cancer

Introduction

Microtubule dynamics is absolutely crucial for the mitotic cell division of the cells. Interference with microtubule dynamics often leads to programmed cell death and thus microtubule-binding drugs are currently used to treat various malignancies in the clinic [1]. Although useful, currently used microtubule drugs such as *Vinca* alkaloids and taxanes are limited due to their undesirable toxicity [2–5]. The wonderful promise of taxol in managing breast cancers justifies further effort to discover novel mitotic inhibitors that may have fewer side effects and that can be easily administered.

CONTACT P.K. Naik pknaik1973@gmail.com
Supplementary data for this article can be accessed at: https://dx.doi.org/10.1080/1062936X.2021.1891567

In quest of finding such a molecule, noscapine (an opium alkaloid, non-narcotic, orally available, safe antitussive drug for over 40 years) was discovered that binds tubulin dimer and arrests the dividing cells in mitosis [6]. However, the cancer cells selectively undergo apoptosis because of the compromised cell cycle check points, without hampering the normal dividing cells. It is well tolerated among healthy volunteers without any significant side effects [7–9]. It has favourable pharmacokinetics in vivo (clearance within ~10 h) [7]. In vitro as well as in vivo mouse xenograft model have shown that noscapine and its analogues are useful in treatment of cancer of different tissues origin [7,10,11]. These properties enable its therapeutic use at high concentrations (~150–300 mg/kg body weight) in murine models of human cancer [11,12]. It is found to inhibiting proliferation and inducing apoptosis in human ovarian carcinoma cell lines that are sensitive or resistant to paclitaxel [13]. The oral bioavailability of noscapine offers further support for its clinical advancement as a novel chemotherapeutic agent [12]. Therefore, noscapine is a promising anticancer drug with minimum toxicity.

Towards improvement of anticancer activity of noscapine, we have developed several of its derivatives. Many of these derivatives were demonstrated to have high tubulin binding and anticancer activity compared to noscapine without any debilitating toxicities [11–16]. In this study, we approach to develop 9-arylimino congeners of noscapine by strategically modifying its scaffold structure; followed by screening of the most potent derivatives based on their predictive binding affinity with tubulin. The screened out derivatives were then chemically synthesized and validated their anticancer activity based on cellular study using two human breast cancer cell lines (MCF-7 and MDAMB-231) and a panel of primary breast tumour cells. The novel derivatives were found to bind tubulin heterodimer with increased binding affinity, effectively inhibit proliferation of cancer cells, selectively arrest cancer cells at G2/M phase and induced apoptosis.

Materials and methods

Protein preparation

The crystal structure of amino noscapine-tubulin complex (PDB ID: 6Y6D, resolution 2.20 Å [17]) was downloaded from the PDB databank and used for structure based designing of novel derivatives of noscapine. It was prepared using protein preparation wizard workflow (Schrödinger). Further, an all atom molecular dynamics (MD) simulation of 100 ns in explicit water was performed to refine the structure using GROMACS 4.5.4 software [18] and the GROMOS96 force field with similar parameters as reported earlier [19]. Finally, the last 2000 frames from the MD trajectory were used to generate an average structure of the tubulin.

Rational design of 9-arylimino congeners of noscapine

We envisaged developing a library of 9-arylimino derivatives of noscapine by hybridizing with arylimino groups (Schiff bases) as depicted in Figure 1. It is because Schiff base analogues have been used in the pharma industry to develop potential

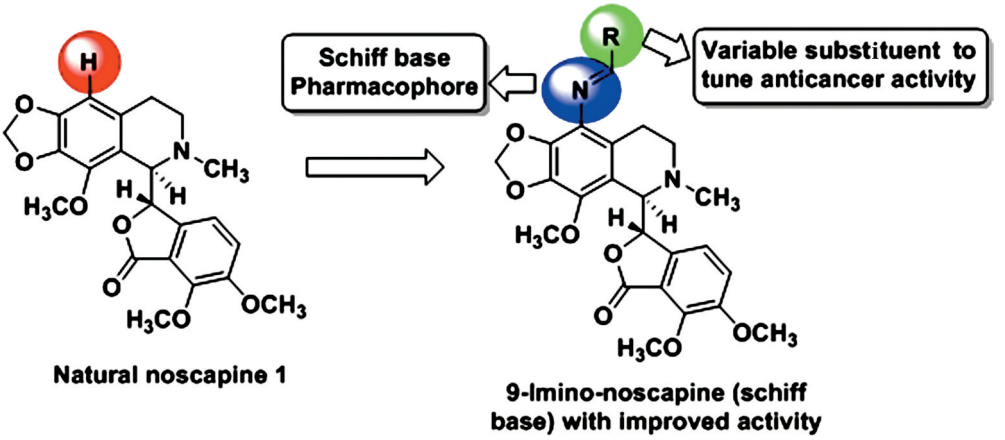

Figure 1. Strategic development of 9-arylimino noscapinoids by hybridizing Schiff base with natural noscapine.

analogues for anticancer activity. As an example, Schiff bases obtained from coumarin and pyrazole aldehyde have been tested against cancer cell lines that showed mild anticancer activities [20]. Furthermore, mono and bis-Schiff bases have been reported efficacious against five cancer cell lines [21].

Preparation of molecular structure

Molecular structures of previously reported noscapinoids [15,16,22–24] (Figure 2) and the newly designed 9-arylimino derivatives of noscapine (Figure 1) were built using ChemDraw. These structures were imported into Maestro (Schrödinger package) and were energy minimized using Macromodel (Schrödinger package) and OPLS 2005 force field with PRCG algorithm (energy gradient of 0.001). The molecular structures were further refined through geometric optimization using hybrid density functional theory with Becke's three-parameter exchange potential and the Lee-Yang-Parr correlation functional (B3LYP) with basis set 3–21 G* using Jaguar (Schrödinger, package). The appropriate bond order for each structure was defined and their various conformations were generated using Ligprep (Schrödinger package).

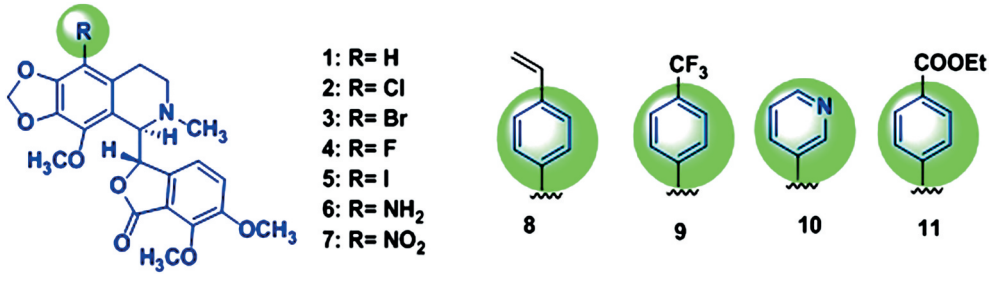

Figure 2. The molecular structure of noscapine and its previously reported derivatives 2–11 used as training set for the molecular modelling study.

Molecular docking

Molecular docking of noscapinoids with αβ-tubulin heterodimer was performed using Glide docking (Schrödinger package) [25,26]. Briefly, the binding site was defined using a concentric grid box at the centroid of the binding site by selecting the co-complex ligand, amino-noscapine using Glide grid-receptor generation program. An outer grid box of 12 Å x 12 Å x 12 Å was defined to confine the mass centre of the docked ligand. Besides an enclosing grid box of 12 Å x 12 Å x 12 Å was defined which occupied all the atoms of the docked poses. The scale factor of 0.4 for van der Waals radii was applied to atoms of protein with absolute partial charges less than or equal to 0.25. The algorithm generated 10000 poses, out of which only 1000 poses were used for the minimization (conjugate gradients) and the final 30 structures having the lowest energy conformations were evaluated for the favourable Glide docking score. All the molecules were docked using Glide XP (extra precision) and evaluated using a Glide XP_{Score} function. The single best conformation for each ligand was considered for molecular dynamics (MD) simulation and predicting the binding affinity.

LIE-SGB model building

A predictive model was developed based on linear interaction energy model (LIE) with a surface generalized Born (SGB) continuum solvation model [27] to calculate the free energy of binding ($\Delta G_{bind,pred}$) of the newly designed 9-arylimino noscapinoids with tubulin. The LIE method employs experimental free energy of binding ($\Delta G_{bind,expt}$) for a training data set of noscapinoids (Figure 2) to estimate the $\Delta G_{bind,pred}$ for the novel set of molecules. The method is based on the linear response approximation, which indicates that free energy of binding of a protein-ligand system is a function of polar and non-polar energy components that scale linearly with the electrostatic and van der Waals interactions between a ligand and its environment. The free energy of binding for the complex is derived from considering only two states: (1) free ligand in the solvent and (2) ligand bound to the solvated protein. The conformational changes and entropic effects pertaining to unbound receptor are taken into account implicitly and only interactions between the ligand and either the protein or solvent are computed during molecular mechanics calculations. The SGB-LIE method used in the study is based on the original formulation proposed by Jorgensen [27] and is implemented in Liaison (Schrodinger package). It also offers better accuracy in treating the long-range electrostatic interactions. The empirical relationship used by LIE-SGB model is shown below.

$$\Delta G_{bind,pred} = \alpha\left(\left\langle U^{b}_{vdw}\right\rangle - \left\langle U^{f}_{vdw}\right\rangle\right) + \beta\left(\left\langle U^{b}_{coul}\right\rangle - \left\langle U^{f}_{coul}\right\rangle\right) + \gamma\left\langle U^{b}_{rxn}\right\rangle - \left\langle U^{f}_{rxn}\right\rangle + \delta\left(\left\langle U^{b}_{cav}\right\rangle - \left\langle U^{f}_{cav}\right\rangle\right)$$

Here $\langle\rangle$ represents the ensemble average, *b* represents the bound form of the ligand, *f* represents the free form of the ligand, α, β, γ and δ are the coefficients of various energy terms, such as van der Waals (U_{vdw}), Coulombic (U_{coul}), reaction field (U_{rxn}) and cavity energy (U_{cav}) in the SGB continuum solvent model. The cavity energy term is proportional to the exposed surface area of the ligand. Thus, the difference in cavity energy between

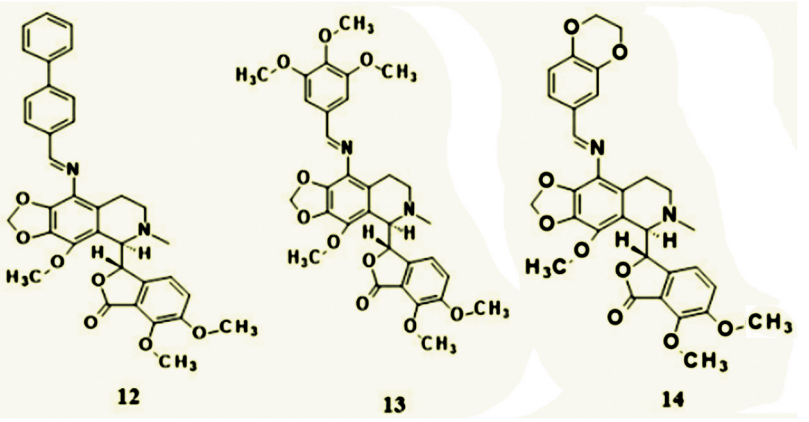

Figure 3. A panel of 9-arylimino noscapinoids, 12–14 that are rationally designed and screened out to have higher binding affinity with tubulin for chemical synthesis and experimental evaluation.

the free and bound form of the ligand measures the surface area lost by contact with the receptor. In the SGB model of solvation, there is no explicit van der Waals or electrostatic interaction between the solute and solvent. The contribution for net free energy of solvation comes from two energy terms, namely, reaction field energy (U_{rxn}) and cavity energy (U_{cav}): $U_{SGB} = U_{rxn} + U_{cav}$. The cavity and reaction field energy terms implicitly take into account the van der Waals and the electrostatic interactions between the ligand and solvent. The above energy parameters from the docked complexes of the noscapinoids were computed based on Hybrid Monte Carlo simulation technique as reported previously [22]. The values of the coefficients were determined based on multiple linear regression techniques without intercept using Minitab statistical package (Minitab Inc.). The $\Delta G_{bind,expt}$ of noscapinoids of the training set with tubulin was calculated from their respective dissociation constant (K_d) values using the relation:

$$\Delta G_{bind,expt} = RT\ ln\ K_d$$

where R is gaseous constant (0.001986 kcal/mol) and T is temperature (298 K).

Finally, based on the docking score and the predictive free energy of binding, we have screened out three most potent 9-arylimino noscapinoids (Figure 3) having enhanced binding affinity with tubulin compared to noscapine for chemical synthesis and cellular evaluation to determine their anticancer potential.

Molecular dynamics simulations

Co-complex of tubulin and 9-arylimino derivatives 12–14 were used for the MD simulation using Amber 16 suite [28]. The parameters for the ligands were estimated using Antechamber program of Amber 16 suite [29]. All atomic point charges were calculated using AM1-BCC charge model [30]. Topologies and internal coordinates for all complexes were generated using tleap program in Amber16. Each molecular system was neutralized by adding counter-ions and was subsequently solvated using TIP3P water model in a truncated octahedron with the distance of 12 Å

between the atoms of protein and wall of the box [31]. Three rounds of minimization were performed on each complex to relax the system and amend the bad contacts. Position restraints of 10 kcal/Å^2 and 2 kcal/Å^2 were imposed on the protein system for the first and the second round, respectively, to relax the water molecules around protein. No restraints were imposed in the third round. The molecular systems were equilibrated at 300 K and 1 atm for 500 ps. The equilibrated systems were then run for 100 ns each with time step of 2 fm. Throughout simulations, the cut-off for non-bonded interaction was 10 Å, electrostatics were calculated using Particle Mesh Ewald (PME) and bonds were constrained using shake algorithm [32–34]. Langevin thermostat was used to regulate the temperature of simulations. Co-ordinates were written every 20 ps to write 5000 frames for each molecular system. CPPTAJ implemented in Ambertools was used to analyse trajectories for root mean square deviation analyses.

Predictive binding affinity

Predicted binding affinity ($\Delta G_{bind,pred}$) of 9-arylimino derivatives 12–14 with tubulin was calculated using Molecular Mechanics Poisson-Boltzmann Surface Area (MM-PBSA) as the ensemble average of the binding free energy of a total of 1000 snapshots, extracted every 20 ps from the last 20 ns of the MD simulation trajectory [35] as explained below:

$$\Delta G_{bind,pred} = \Delta G_{complex} - \left[\Delta G_{Rec} + \Delta G_{lig}\right]$$
$$G = E_{gas} + G_{sol} - TS.$$
$$E_{gas} = E_{int} + E_{ele} + E_{vdw}$$
$$G_{sol} = G_{PB(GB)} + G_{sol-np}$$
$$G_{sol-np} = \gamma SAS$$

where G is Gibbs free energy, E_{gas} is the gas phase energy calculated as the sum of internal energy (E_{int}), energy generated as a result of the electrostatic interaction (E_{ele}) and the van der Waals interaction (E_{vdw}). G_{sol} is the solvation free energy calculated as the sum of polar ($G_{PB(GB)}$) and non-polar contributions ($G_{sol\text{-}np}$). Polar interaction contribution ($G_{PB(GB)}$) was calculated as the summation of electrostatic contribution (E_{ele}) and polar solvation contribution ($G_{PB(GB)}$). The non-polar solvation contribution ($G_{sol\text{-}np}$) is approximated as linearly dependent on the solvent accessible surface area (SAS) and γ is the surface tension constant that was set to 0.0072 kcal mol^{-1} Å $^{-2}$.

Chemical synthesis of 9-arylimino derivatives 12–14

Chemical synthesis of the derivatives of noscapine is very difficult due to highly sensitive C-C bond between isoquinoline and isobenzofuranone ring components which is labile to strong acids and base. However, we have strategically designed the synthetic scheme (Figure 4) for the amalgamation of the 9-arylimino derivatives 12–14 from noscapine as starting material without affecting the sensitive C-C bond. Briefly, the natural α-noscapine was converted to 9-aminonoscapine via two reaction steps involving bromination of noscapine using aqueous HBr/Br_2-H_2O followed by amination using CuI, NaN_3 and L-Proline in DMSO as reported earlier [14]. A solution of 9-aminonoscapine #6 (1.0 mmol), in ethanol (15 mL) was refluxed with substituted

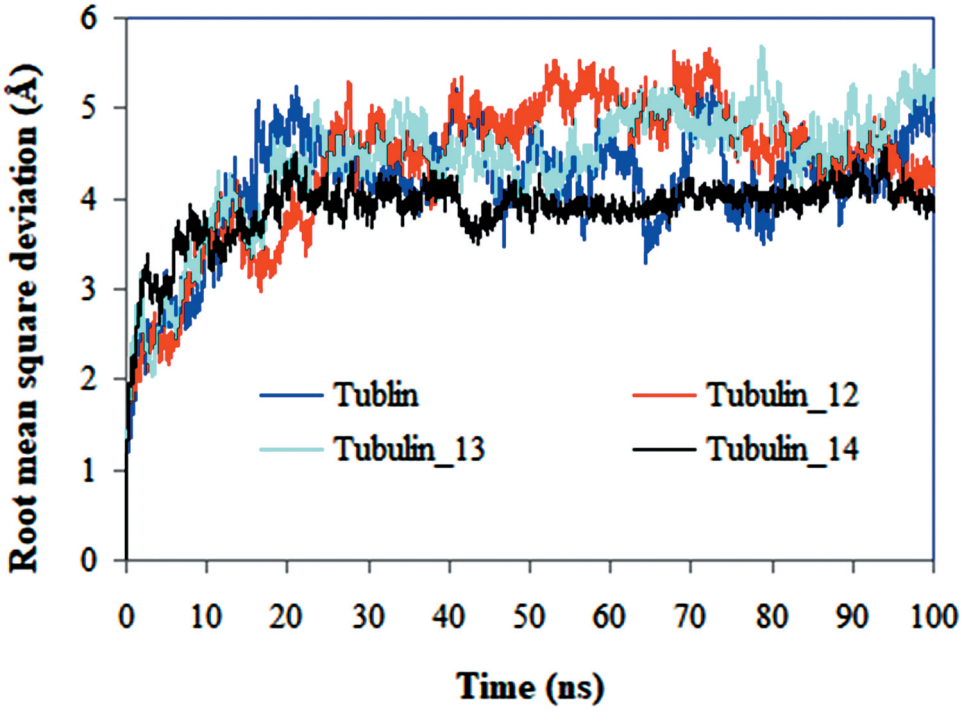

Figure 4. General chemical reaction for chemical synthesis of 9-arylimino noscapinoids 12–14, rationally designed in the study. Reaction conditions: (i) 48% HBr, Br_2-water, rt, 2 h (ii) CuI, NaN_3, L-Proline, DMF, 140°C, 4 h, (iii) RCHO, EtOH, reflux, 24 h.

aryl/heteroaryl aldehydes (2,5-difluorobenzaldehyde or 5-bromothiophene- carboxaldehyde or *p*-bromo benzaldehyde, 1.0 mmol), for 12 h. The crude residue was chromatographed over a triethylamine silica bed, using pet.ether/ethyl acetate (7:3) as eluents to produce 9-arylimino noscapinoids 12–14 (Figure 4) as solid products in very good yield. The details of chemical synthesis and the structural characterization by ^{1}H, ^{13}C NMR and mass (ESI and HRMS) spectral data of 9-arylimino derivatives 12–14 were included in supporting material.

Structural characterization of 9-arylimino noscapinoids, 12–14

(S)-3-((R)-9-((E)-([1,1′-biphenyl]-4-ylmethylene)amino)-4-methoxy-6-methyl-5,6,7,8-tetrahydro-[1,3]dioxolo[4,5-g]isoquinolin-5-yl)-6,7-dimethoxyisobenzofuran-1(3 H)-one (12)

Nature: White solid. mp: 95–97°C. IR (KBr): 3447, 2933, 1759, 1626, 1491, 1436, 1384, 1122, 1033, 969, 840, 763, 695 cm-1. 1 H NMR (400 MHz, CDCl3): δ 8.90 (s, 1 H, N = CH), 7.96 (d, *J* = 8.3 Hz, 2H, Ar-H), 7.69 (d, *J* = 8.3 Hz, 2 H, Ar-H), 7.65 (d, *J* = 7.2 Hz, 2 H, Ar-H), 7.50–7.44 (m, 2 H, Ar-H), 7.39 (t, *J* = 7.3 Hz, 1 H, Ar-H), 7.00 (d, *J* = 8.3 Hz, 1 H, Ar-H), 6.32 (d, *J* = 8.3 Hz, 1 H, Ar-H), 6.00 (dd, *J* = 1.3, 16.2 Hz, 2 H, O-C*H*2-O), 5.59 (d, *J* = 4.2 Hz, 1 H, Ar-CH, (C3-phthalide)), 4.40 (d, *J* = 4.2 Hz, 1 H, Ar-CH, (C5′-isoquinoline)), 4.10 (s, 3 H, -OCH3), 4.05 (s, 3 H, -OCH3), 3.86 (s, 3 H, -OCH3), 3.05–2.97 (m, 1 H, -C*H*H-*N*-CH3 (C7′-

isoquinoline)), 2.74–2.66 (m, 1 H, -CH*H*-*N*-CH3 (C7′-isoquinoline)), 2.56 (s, 3 H, *N*-C*H*3), 2.45–2.38 (m, 1 H, Ar-C*H*H (C8′-isoquinoline)), 2.09–2.00 (m, 1 H, Ar-CH*H* (C8′-isoquinoline)). 13 C NMR (100 MHz, CDCl3): δ 168.1, 161.2, 152.1, 147.6, 143.7, 141.3, 140.2, 139.1, 138.7, 135.8, 134.5, 130.1, 129.1, 128.8, 128.7, 127.7, 127.2, 125.8, 119.8, 118.3, 117.7, 100.8, 81.8, 62.2, 59.4, 56.7, 49.4, 45.9, 22.8. MS (ESI-MS) *m/z*: 593 [M + H]+ HRMS (ESI): Calcd for C35H33N2O7 [M + H]+: 593.22823, found: 593.22731.

(S)-6,7-dimethoxy-3-((R)-4-methoxy-6-methyl-9-((E)-(3,4,5-trimethoxybenzylidene) amino)5,6,7,8-tetrahydro-[1,3]dioxolo[4,5-g]isoquinolin-5-yl)isobenzofuran-1(3 H)-one (13)

Nature: White solid. mp: 124–126°C. IR (KBr): 3493, 2952, 2899, 2843, 2794, 1758, 1628, 1580, 1499, 1459, 1390, 1275, 1122, 1037, 1006, 975, 846, 798, 727 cm-1. 1 H NMR (400 MHz, CDCl3): δ 8.73 (s, 1 H, N = CH), 7.15 (s, 2 H, Ar-H), 7.01 (d, *J* = 8.3 Hz, 1 H, Ar-H), 6.35 (d, *J* = 8.3 Hz, 1 H, Ar-H), 5.99 (dd, *J* = 1.3, 16.0 Hz, 2 H, O-CH2-O), 5.58 (d, *J* = 4.4 Hz, 1 H, Ar-CH, (C3-phthalide)), 4.39 (d, *J* = 4.4 Hz, 1 H, Ar-CH, (C5′-isoquinoline)), 4.10 (s, 3 H, -OCH3), 4.03 (s, 3 H, -OCH3), 3.94 (s, 6 H, 2 x – OCH3), 3.91 (s, 3 H, -OCH3), 3.86 (s, 3 H, –OCH3),3.01–2.91 (m, 1 H, -C*H*H-*N*-CH3 (C7′- isoquinoline)), 2.75–2.67 (m, 1 H, -CH*H*-*N*-CH3 (C7′- isoquinoline)), 2.55 (s, 3 H, *N*-C*H*3), 2.47–2.39 (m, 1 H, Ar-C*H*H (C8′-isoquinoline)), 2.09–2.00 (m, 1 H, Ar- CH*H* (C8′-isoquinoline)). 13 C NMR (100 MHz, CDCl3): δ 168.1, 161.4, 153.4, 152.1, 147.6, 141.4, 140.8, 138.9, 138.6, 134.5, 132.3, 128.6, 125.8, 119.8, 118.4, 117.7, 105.3, 100.8, 81.7, 62.2, 60.9, 59.5, 56.7, 56.1, 54.8, 49.3, 45.8, 22.6. MS (ESI-MS) *m/z*: 607 [M + H]+ HRMS (ESI): Calcd for C32 H35N2O10 [M + H]+: 607.22862, found: 607.22803.

(S)-3-((R)-9-((E)-((2,3-dihydrobenzo[b][1,4]dioxin-6-yl)methylene)amino)-4-methoxy-6-methyl 5,6,7,8-tetrahydro-[1,3]dioxolo[4,5-g]isoquinolin-5-yl)-6,7-dimethoxyiso benzofuran-1(3 H)-one (14)

Nature: White solid. mp: 155–157 oC. IR (KBr): 3423, 2928, 2796, 1759, 1629, 1578, 1430, 1383, 1294, 1268, 1068, 1034, 1007, 971, 885 cm-1. 1 H NMR (400 MHz, CDCl3): δ 8.71 (s, 1 H, N = CH), 7.46 (d, *J* = 1.9 Hz, 1 H, Ar-H), 7.36 (dd, *J* = 1.9, 8.4 Hz, 1 H, Ar-H), 6.98 (d, *J* = 8.1 Hz, 1 H, Ar-H), 6.93 (d, *J* = 8.3 Hz, 1 H, Ar-H), 6.27 (d, *J* = 8.1 Hz, 1 H, Ar-H), 5.98 (dd, *J* = 1.3, 15.5 Hz, 2 H, O-C*H*2-O), 5.58 (d, *J* = 4.2 Hz, 1 H, Ar-CH, (C3-phthalide)), 4.39 (d, *J* = 4.2 Hz, 1 H, Ar-CH, (C5′- isoquinoline)), 4.34–4.28 (m, 4 H, O-C*H*2-C*H*2-O), 4.10 (s, 3 H, -OCH3), 4.03 (s, 3 H, -OCH3), 3.86 (s, 3 H, -OCH3), 2.99–2.90 (m, 1 H, -C*H*H-*N*-CH3 (C7′-isoquinoline)), 2.70–2.62 (m, 1 H, -CH*H*-*N*-CH3 (C7′-isoquinoline)), 2.54 (s, 3 H, *N*-C*H*3), 2.42–2.33 (m, 1 H, Ar-C*H*H (C8′-isoquinoline)), 2.02–1.92 (m, 1 H, Ar-CH*H* (C8′-isoquinoline)). 13 C NMR (100 MHz, CDCl3): δ 168.1, 161.0, 152.1, 147.6, 146.4, 143.7, 141.3, 138.9, 138.4, 134.6, 130.8, 128.8, 125.9, 122.4, 119.9, 118.2, 117.7, 117.6, 117.4, 116.6, 100.8, 81.8, 64.5, 64.1, 62.2, 60.9, 59.5, 56.7, 49.5, 45.9, 22.8. MS (ESI-MS) *m/z*: 575 [M + H]+ HRMS (ESI): Calcd for C31 H31N2O9 [M + H]+: 575.20241, found: 575.20129.

Tubulin purification

Microtubules were isolated and purified from the goat brain through alternative cycles of GTP-dependent polymerization and depolymerization in PEM buffer (50 mM pipes, 3 mM MgSO4, 1 mM EGTA, pH 6.8) [36,37]. The purified microtubules were preserved at −80°C. The purified tubulin was estimated using the Bradford method as well as by SDS PAGE [38].

Tubulin binding assay using tryptophan quenching

Tubulin (2 μM) was incubated in a water bath with 9-arylimino noscapinoids 12–14 at a concentration of 25 μM in PEM buffer (50 mM pipes, 3 mM MgSO4, 1 mM EGTA, PH 6.8) for 45 min at 35 °C. The samples were excited at 295 nm and emission was measured at 310–400 nm. For the spectrofluorometric titrations, a FlouroMax ® 4 spectrofluorometer (Horiba Scientific, Edison, NJ) assisted by Fluor Essence 3.5 software was used. The experiments were repeated twice.

Cellular proliferation using MCF-7 and MDAMB-231 cell lines

Antiproliferation activity of 9-arylimino noscapinoids, 12–14 was performed in 96-well plates as described previously using two human breast cancer cell lines, MCF-7 and MDAMB-231 [23]. In brief, cells were grown in DMEM culture medium supplemented with 10% FBS, 1% penicillin/streptomycin and 2 mM l-glutamine at 37°C in a humidified atmosphere with 5% CO_2. Cells were plated at a density of 5×10^3 cells per well and were treated with gradient concentrations (5 to 100 μM) of noscapine and its derivatives, 12–14 for 72 h. Measurement of cell proliferation was performed by sulforhodamine B (SRB) assay, using the CellTiter96 AQueous One Solution Reagent (Sigma). The IC_{50} value that stands for the drug concentration required to achieve a cell kill of 50% was determined using the online tool Quest GraphTM IC_{50} Calculator (AAT Bioquest, Inc., Sunnyvale, CA, USA, https://www.aatbio.com/tools/ic50-calculator).

Primary breast cancer cells (PBCs) culture and in vitro cell proliferation assay

Primary breast cancer cells were isolated from the patient's samples (8 nos.) with different stages of breast cancer before drug treatment in aseptic condition. The tumour tissues were treated with 0.25% trypsin and filtered with 70-micron filter followed by centrifugation at 2000 rpm for 3 minutes with serum-free medium. The filtered cells were collected and plated in T25 flask and incubated with complete DMEM culture medium, supplemented with 10% FBS and 1% pentrip (mixture of penicillin and streptomycin) at 37°C under 5% CO_2. Fresh media was replaced every 3–4 days, and subsequent passages were performed under the same conditions as mentioned above. The cultures were maintained for homogeneous cell type at sub-confluence between 3 and 8 passages. Cells were allowed to reach 80–90% confluence prior to experimental treatments. After the confluence reached the desired level, the primary cells were plated at 2000 cells/well in 96 wells plate with culture media. The cells were maintained at 37°C in a humidified atmosphere with 5% CO_2 and were treated with gradient concentrations (5 to 100 μM) of noscapine and 9-arylimino noscapinoids, 12–14 for 72 h. Measurement of cell proliferation was performed by sulforhodamine B (SRB) assay, using the CellTiter96 AQueous One Solution Reagent (Sigma). Cells were stained with SRB for 30 minutes. The unbound dye was removed by washing. The bound dye was extracted with 1 mM tris and absorbance was measured using a SPECTRAmax PLUS 384 microplate spectrophotometer at 564 nm. The percentage of cell survival as a function of drug concentration was plotted and the IC_{50} value was determined using the online tool, AAT Bioquest.

Analysis of cell cycle progression

Inhibition of cell cycle progression with the treatment of 9-arylimino noscapinoids 12–14 was investigated using MDAMB-231 cells. The cells were maintained in DMEM culture media with 4.5 g/L glucose and L-glutamine supplemented with 10% FBS and 1% penicillin/streptomycin, at 37°C in a 5% CO_2 atmosphere. After reaching the 80–90% confluence, cells were treated with noscapine and 9-arylimino noscapinoids, 12–14 dissolved in 1% phosphate buffer saline (PBS). After 72 h of treatment, cells were harvested and analysed using flow cytometry. Briefly, 2×10^6 cells were centrifuged, washed twice with ice-cold PBS and fixed in 70% ethanol at −20°C for 24 h. The cells were centrifuged at 1000 x g for 10 min and the supernatant was discarded. The pellet was resuspended in 30 µl of phosphate/citrate buffer (0.2 M Na_2HPO_4/0.1 M citric acid, pH 7.5) at room temperature for 30 min. The cells were washed with 5 ml of PBS, incubated with 0.5 ml of propidium iodide (20 µg/ml in 0.6% Triton-X in PBS) and 0.5 ml of RNase A (20 µg/ml in PBS) for 45 min. in dark. Samples were analysed on a flow cytometer (BD FACS Aria-III) and the progress in the cell cycle was determined.

Apoptosis assay

Apoptosis in cancer cells was detected by Annexin-V-FITC apoptosis detection method by using Apoptosis detection kit (Sigma–Aldrich, USA) based on instruction provided by the manufacturer. For experimental purpose, 3×10^4 cells per well were seeded on 12 well culture plate and incubated for 24 h with complete medium. The cells were treated with IC_{50} concentration of noscapine and 9-arylimino noscapinoids, 12–14 and were harvested at 72 h. Cells were typsinized and stained with surface marker antibodies (biotin-conjugated Annexin V, FITC-conjugated streptavidin) and propidium iodide (PI) in 1X binding buffer for 20 min in dark condition at room temperature. Flow cytometer data with 488 nm excitation for PI and emission at 530 nm were collected. Viable cells (Annexin V^-/PI^-), early apoptotic cells (Annexin V^+/PI^-), late apoptotic/necrotic cells (Annexin V^+/PI^+) and late necrotic cells (Annexin V^-/PI^+) were identified and their percentage was determined.

DAPI staining

Apoptotic cancer cells were visualized by fluorescence microscopy following DAPI staining. Briefly, MDAMB-231 cells were grown on poly-L-lysine coated coverslips in 6-well plates and were treated with test molecules at 25 µM for 72 h. After incubation, cover slips were fixed in cold methanol, washed with PBS, stained with DAPI and mounted on slides. Images were captured using a fluorescent microscope (Nikon Eclipse Ts2R-FL). Apoptotic cells were identified by alterations of morphological features (e.g. nuclear condensation, formation of membrane blebs and apoptotic bodies).

Results and discussion

After the establishment of anticancer activity of the lead molecule, noscapine, several derivatives have been developed by various groups in order to increase its therapeutic

outcome. Many of these derivatives were demonstrated to have higher binding affinity with tubulin, antiproliferative activity and induction of apoptosis. As an example, the tubulin-binding affinity and antiproliferative activity have been increased by 20 to 80 folds through developing halogenated, nitro, amino and biaryl noscapinoids by modification at C-9 position of the scaffold [22,24,39,40] as well as by functionalization of 'N' in isoquinoline unit of natural α-noscapine [41]. Structure-activity data of these derivatives of noscapine led us to develop a reasonable predictive model for predicting the free energy of binding of newly designed derivatives and screening of promising derivatives. We are reporting in this study a panel of 9-arylimino noscapinoids, 12–14 as potent anticancer agents.

Molecular docking and binding affinity of 9-arylimino noscapinoids with tubulin

The library of 9-arylimino noscapinoids designed in the study and the training set molecules were docked onto the binding site of tubulin dimmer and were ranked based on their docking score. The docked complexes were then used for hybrid Monte Carlo simulation with SGB continuum solvation model to calculate the various interaction energy terms (van der Waals energy (U_{vdw}), Coulombic energy (U_{coul}), reaction energy (U_{rxn}) and cavity energy (U_{cav})) using Liaison (Schrodinger). These energy parameters of the training set molecules (Table 1) were mapped with their experimental free energy of binding ($\Delta G_{bind,expt}$) through linear regression technique to develop the robust prediction model for predicting the $\Delta G_{bind,pred}$ of the noscapinoids with tubulin. The values obtained for the four fitting parameters, α, β, γ and δ are 0.08446, −0.00223, −0.000872 and −0.45601, respectively. The $\Delta G_{bind,pred}$ of the training set molecules based on LIE-SGB model is very close to the $\Delta G_{bind,expt}$ (root mean square error was 0.243 kcal/mol) (Table 1). The quality of the fit can also be judged by the value of the coefficient of determination (r^2) and analysis of variance (F-value).

$$\Delta G_{bind,pred} = 0.08446U_{vdw} - 0.00223U_{coul} - 0.00872U_{rxn} - 0.45601U_{cav}$$

$$n = 11, r^2 = 0.998, s = 0.243, F = 3742.6, p \leq 0.001$$

Because of high predictability, the LIE-SGB model was used to predict the binding free energy of the newly designed 9-arylimino noscapinoids. Based on the improved docking score and predicted binding free energy compared to noscapine (Table 1) we have selected three molecules, 12–14 for chemical synthesis and experimental evaluation.

MD simulation of co-complexes of molecules with tubulin

The complexes of 9-arylimino noscapinoids, 12–14 and tubulin obtained after molecular docking were simulated for 100 ns to obtain a total of 10,000 frames. The stability of the system was monitored by means of RMSD of Cα-atoms during the entire duration of simulation as shown in Figure 5. All the systems observed to get stabilized after 20 ns of simulation, since the relative fluctuation in the RMSD of Cα carbon atoms (Cα-rmsd) is very small after equilibration. Overall, the RMSD ranges from 0 to 2.582 Å. Furthermore, root mean square fluctuations (RMSF) of Cα-atoms were also calculated for all the systems to find any changes in the residue

Table 1. Molecular docking results (Glide XP) as well as calculated energies using Liasion programme (Schrodinger package) of noscapine and its derivatives: van der Waals energy (U_{vdw}), Coulombic energy (U_{coul}), reaction energy (U_{rxn}) and cavity energy (U_{cav}) as well as predicted free energy of binding ($\Delta G_{bind,pred}$) based on LIE-SGB prediction model and experimental free energy of binding ($\Delta G_{bind,expt}$). The newly designed 9-arylimino noscapinoids, 12–14 revealed improved $\Delta G_{bind,pred}$ compared to the lead molecule, noscapine.

Ligand	*Glide XP_{score} (kcal/mol)*	*<U_{vdw}> (kcal/mol)*	*<U_{coul}> (kcal/mol)*	*<U_{rxn}> (kcal/mol)*	*<U_{cav}> (kcal/mol)*	*$\Delta G_{bind,\ expt}$ (kcal/mol)*	*$\Delta G_{bind,\ pred.}$ (kcal/mol)*
1	−1.927	−45.14	−330.8	135.5	2.097	−5.246	−5.212
2	−2.038	−49.00	−210.2	116.0	3.283	−6.006	−6.178
3	−2.766	−42.50	−362.1	155.9	4.208	−5.827	−6.060
4	−2.940	−48.06	−355.8	168.7	2.548	−5.587	−5.899
5	−3.263	−47.69	−285.7	135.5	3.103	−6.360	−5.987
6	−4.492	−47.44	−77.3	118.2	3.954	−6.628	−6.668
7	−2.605	−33.39	−331.9	176.7	4.465	−5.551	−5.657
8	−2.287	−45.57	−277.9	112.3	3.285	−5.665	−5.706
9	−2.350	−33.47	−324.5	152.5	3.766	−5.783	−5.151
10	−3.679	−45.41	−471.2	152.8	3.669	−5.673	−5.790
11	−4.687	−42.69	−267.6	129.9	3.465	−5.518	−5.722
12	−2.918	−40.60	−233.8	120.6	3.134	-	−5.390
13	−3.948	−46.67	−318.1	141.7	4.468	-	−6.506
14	−4.433	−45.05	−286.4	129.6	5.224	-	−6.679

<U_{vdw}>, <U_{coul}>, <U_{rxn}> and <U_{cav}> energy terms represents the ensemble average energy terms calculated as the difference between bound and free state of the ligands and its environment. Experimental ΔG_{bind} was calculated from the dissociation constant (K_d value) using the relationship: $\Delta G_{bind} = RTlnK_d$ where T = 298 K and R = 0.00199 (kcal/mol.K). Predicted ΔG_{bind} was calculated using linear interaction energy (LIE) empirical equation:

$$\Delta G_{bind,pred} = 0.08446U_{vdw} - 0.00223U_{coul} - 0.00872U_{rxn} - 0.45601U_{cav}$$

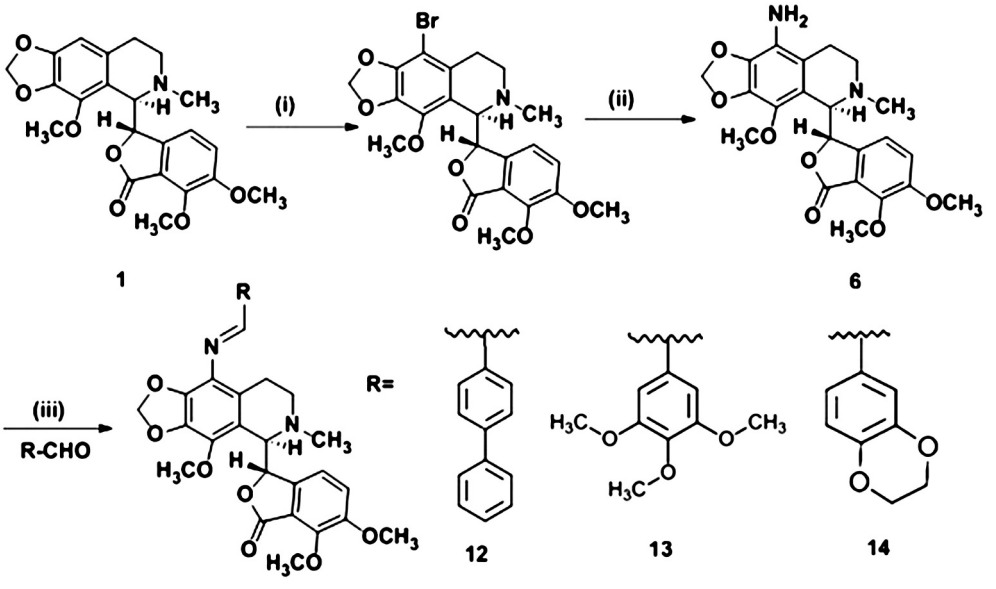

Figure 5. Root mean square deviations (RMSD) of Cα carbon atoms of tubulin only and in complex with 9-arylimino noscapinoids 12–14 during 100 ns of MD simulation. The relative fluctuation in the RMSD of the Cα atoms is very small after ~20 ns of the simulation. The time step of 20 ps was used during the simulation that generated 5,000 frames which were used to generate the average structure.

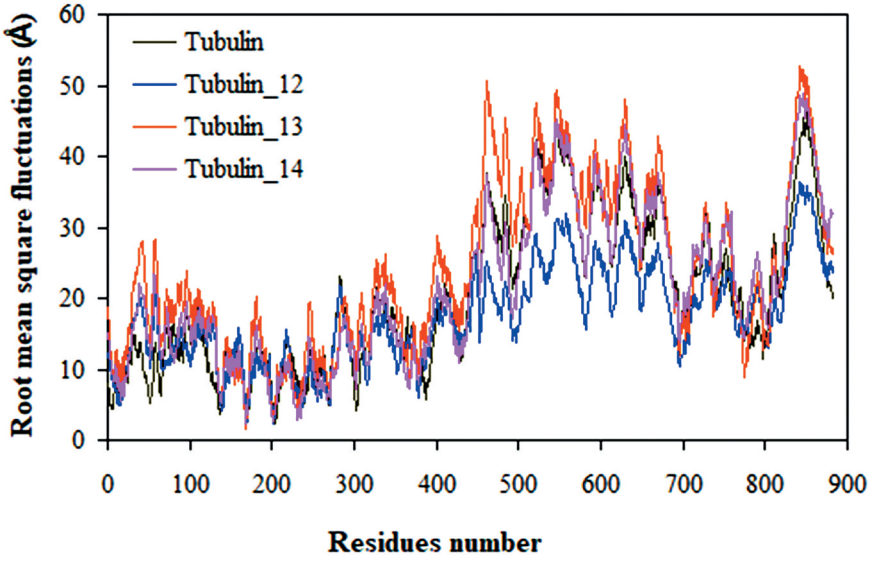

Figure 6. Root mean square fluctuation (RMSF) of the residues of tubulin of the docked ligands in the bound form and in the unbound form of tubulin heterodimer. Different levels of flexibility of these residues were noticed in the bound form of tubulin with 9-arylimino noscapinoids 12–14.

flexibilities. The RMSF values were plotted against residue numbers based on the 100 ns trajectory as shown in Figure 6. The residues with higher RMSF tend to show more flexibility. The molecules 12–14 were observed to bind with the tubulin throughout the simulation. They were found to accommodate well inside the binding cavity (Figure 7) at the interface between α- and β- tubulin. Their mode of interaction with the binding site amino acids is depicted as ligplot (Figure 7). It explains the formation of different hydrogen bonds and hydrophobic interactions between the ligands and the binding site amino acids.

Predicted binding free energy of 9-arylimino noscapinoids with tubulin

Predicted binding free energy ($\Delta G_{bind,pred}$) of 9-arylimino noscapinoids, 12–14 with tubulin were calculated using MM-PBSA and included in Table 2. Robust binding free energy of −166.03, −169.75 and −170.63 kcal/mol was predicted for the molecules 12, 13 and 14, respectively. For all complexes, the binding free energy was decomposed into its various energy components (the electrostatic, van der Waals and solvation). Both van der Waals (ΔE_{VDW}) and the electrostatic component (ΔE_{ELE}) were observed to make very significant contributions to the free energy of binding. However, the solvation contribution ($\Delta G_{SOL\text{-}PB}$) was rendered unfavourable while the net non-polar component (ΔE_{vdw}) and ($\Delta G_{sol\text{-}np}$) were observed to make highly favourable contribution to the binding free energy.

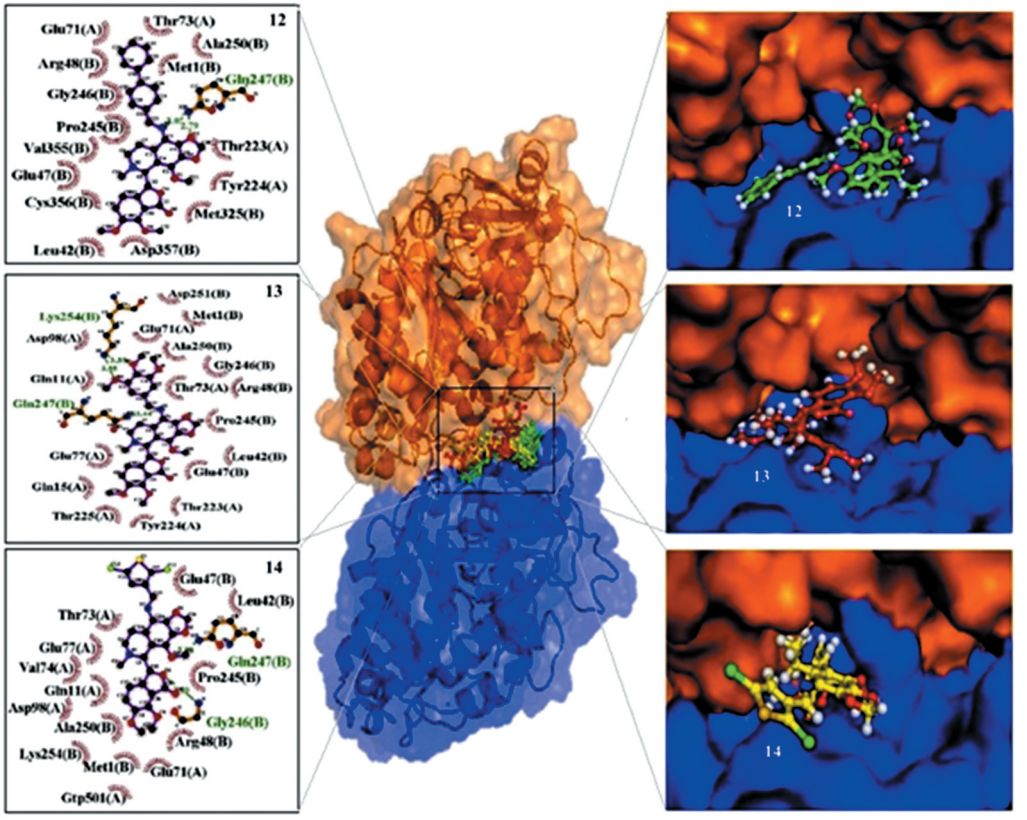

Figure 7. The newly designed 9-arylimino noscapinoids 12–14 are well accommodated inside the noscapine binding site at the interface of α- and β- tubulin. The binding site is represented as macro model surface according to α- and β- tubulin (α-tubulin is represented in blue colour and β-tubulin is represented in brown colour). The ligplot analysis showed the interaction of binding site amino acids with the 9-arylimino noscapinoids 12–14. The binding site residues involved in the interactions are slightly different mainly because of the variation in functional groups. The hydrogen bonds formed (if any) are represented as dotted lines.

Table 2. Calculated binding free energy and its various components (kcal/mol) of 9-arylimino noscapinoids, 12–14 with tubulin. The values in bold represent the ΔG_{bind} energy of molecules with tubulin based on MM-PBSA.

Compound	ΔE_{VDW} *(kcal/mol)*	ΔE_{ELE} *(kcal/mol)*	$\Delta G_{SOL\text{-}PB}$ *(kcal/mol)*	$\Delta G_{SOL\text{-}NP}$ *(kcal/mol)*	$\Delta G_{bind\text{-}PBSA}$ *(kcal/mol)*
Tubulin_12	−31.29	−210.31	79.74	−4.17	−166.03
Tubulin_13	−31.57	−188.54	53.77	−4.30	−170.63
Tubulin_14	−41.81	−177.64	54.53	−4.82	−169.75

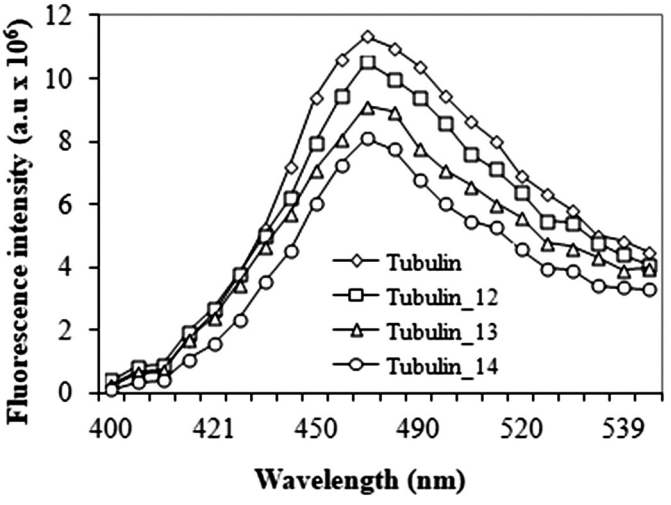

Figure 8. Decrease of fluorescence intensity of tubulin by 9-arylimino noscapinoids 12–14. Tubulin (2.0 μM) was incubated with molecules 12–14 (25 μM) and the emission spectra were collected (310 nm – 400 nm). All the three molecules showed a quenching of the intrinsic tubulin fluorescence emission intensity, indicating their binding to tubulin. The graph is a representative of three independent experiments.

Tubulin binding of 9-arylimino noscapinoids

Tubulin is autofluorescence in nature due to the presence of many tryptophan amino acids. Thus, decrease in emission fluorescence with ligand binding due to alteration in its conformation could be useful in monitoring ligand binding with tubulin. The reduced fluorescence intensity in the value of −5.74%, −15.11%, and −35.97%, respectively, in the presence of 25 μM concentration of 9-arylimino noscapinoids 12–14 indicates binding with tubulin (Figure 8).

9-Arylimino noscapinoids inhibits proliferation of MCF-7 and MDAMB-231

We focused at the cellular level to determine if the 9-arylimino noscapinoids, 12–14, affected cancer cell proliferation. The 9-arylimino noscapinoids 12–14 including the parent compound, noscapine were analysed for their antiproliferative activity in two human breast cancer cell lines, MCF-7 (oestrogen- and progesterone-receptor positive) and MDAMB-231 (oestrogen- and progesterone-receptor negative) (Figure 9). The IC_{50} values of the molecules for both the cell lines are collated in Table 3. The IC_{50}

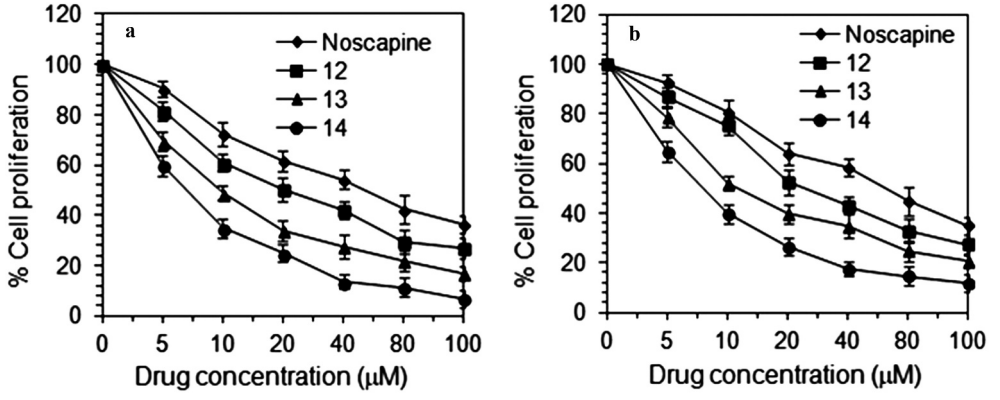

Figure 9. The 9-arylimino noscapinoids 12–14 are more active compared to noscapine in inhibiting the proliferation of human breast cancer cells. Both (A) MCF-7 and (B) MDAMB-231. Cancer cells were treated with noscapine and 9-arylimino noscapinoids, 12–14 for 72 h. Each value represents the average of 3 independent experiments.

Table 3. IC_{50} values of novel 9-arylimino noscapinoids, 12–14 using two human breast adenocarcinoma cell lines, MCF-7 and MDAMB-231. All the novel derivatives were found to have improved antiproliferative activity compared to noscapine.

	IC_{50} (μM)			
	Noscapine	*12*	*13*	*14*
MCF-7	44.8 ± 4.3	23.1 ± 2.1	10.8 ± 1.3	6.4 ± 0.6
MDAMB-231	51.8 ± 5.7	29.2 ± 2.4	14.9 ± 1.2	7.6 ± 0.5

value was found to be 44.8 μM, 23.1 μM, 10.8 μM and 6.4 μM for noscapine, 12, 13 and 14, respectively, for MCF-7 cells, which reflects a modest antiproliferative activity. Similar modest IC_{50} value of 51.8 μM, 29.2 μM, 14.9 μM and 7.6 μM was measured for noscapine, 12, 13 and 14, respectively, for MDAMB-231 cells. The closer IC_{50} values obtained using both cells suggested that the tested molecules inhibit cancer cell proliferation independent of hormone receptor status. Although significant correlation of the sensitivity of cancer cells to these analogues cannot be established at this stage, the study indicated that tubulin represents a potential target for these molecules. The IC_{50} values did not show close correlation among these analogues due to its cell-type dependency.

9-Arylimino noscapinoids inhibits proliferation of primary breast cancer cells

The inhibition of proliferation of primary tumour cells of different stages of breast cancer was evaluated against the newly developed 9-arylimino noscapinoids, 12–14. The study revealed that all the newly designed 9-arylimino noscapinoids exhibited potent cytotoxic activity in comparison to noscapine using all the primary breast tumour cells (Figure 10). The IC_{50} value ranges from 43.6 to 49.8 μM for noscapine, 24.1 to 30.1 μM for #12, 11.7 to 19.9 μM for #13 and 5.8 to 6.9 μM for #14 (Table 4).

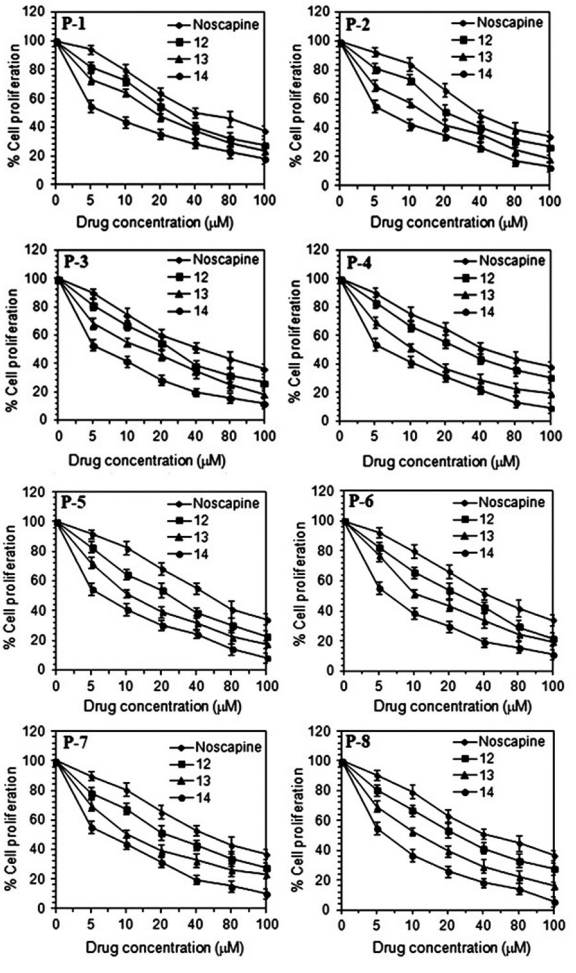

Figure 10. The 9-arylimino noscapinoids, 12–14 are more active compared to noscapine in inhibiting the proliferation of a panel of human primary breast cancer cells. All the cells treated with 9-arylimino noscapinoids, 12–14 for 72 h. Each value represents the average of 3 independent experiments.

Table 4. IC_{50} values of novel 9-arylimino noscapinoids, 12–14 using primary breast cancer cells isolated from breast tumour tissue of different patients. All the derivatives were found to have improved anti-proliferative activity compared to noscapine.

Patients	*IC_{50} (μM)*			
No.	*Noscapine*	*12*	*13*	*14*
1	47.9 ± 5.3	27.7 ± 2.9	19.9 ± 2.4	6.7 ± 0.7
2	43.6 ± 5.7	27.1 ± 2.6	14.9 ± 1.8	6.9 ± 0.5
3	44.2 ± 4.8	25.6 ± 2.7	14.8 ± 2.3	5.9 ± 0.8
4	48.1 ± 4.3	30.1 ± 2.3	11.7 ± 1.3	6.4 ± 0.4
5	49.8 ± 4.9	24.1 ± 2.2	13.2 ± 1.5	6.4 ± 0.6
6	45.8 ± 4.5	25.1 ± 3.1	15.2 ± 1.7	5.9 ± 0.3
7	49.8 ± 4.8	26.3 ± 3.5	12.9 ± 0.8	6.9 ± 0.5
8	47.8 ± 5.2	26.6 ± 2.6	12.5 ± 0.6	5.8 ± 0.4

Table 5. Percentage of early apoptotic (Q1), late apoptotic (Q2), viable (Q3) and necrotic (Q4) cell measured by flow cytometry using MDAMB-231 cells treated with 25 µM solution of 9-arylimino noscapinoids, 12–14 for 72 hours.

Viability/ Apoptotic	*Control*	*Noscapine*	*12*	*13*	*14*
Q1	5%	30%	20%	23%	27%
Q2	2%	10%	30%	36%	39%
Q3	91%	50%	42%	35%	18%
Q4	2%	3%	5%	15%	12%

9-Arylimino noscapinoids induced apoptosis to cancer cells

The induction of apoptotic cell death to breast cancer cell by the 9-arylimino noscapinoids, 12–14 was determined by FACS analysis. Apoptosis of cell is characterized by the alterations in lipid composition of cell membrane. Phosphatidylserine on the inner leaflet of cell membrane translocates to outer leaflet, which can be measured using Annexin V binding. In contrast, the cell impairment DNA binding fluorescent dye, propodium iodide can only enter the cells at the stage of late apoptosis when the membrane permeability is compromised. The percentage of early and late apoptotic cells using MDAMB-231 cell line for treatment of noscapine and its 9-arylimino noscapinoids, 12–14 with a concentration of 25 µM for 72 h is collated in Table 5 and Figure 11. After 72 h of culture, the control untreated cell represented only few early apoptotic (2.5%) and late apoptotic cells (1.0%) due to regular trauma during cell culture, which were considered as the background cell death. In contrast, the percentage of early apoptotic cells of 30%, 20%, 23%, 27%; late apoptotic cells of 10%, 30%, 36%, 39% and necrotic cells of 3%, 5%, 15% and 12% treated with noscapine and its 9-arylimino noscapinoids, 12–14, respectively, were found to be relatively higher compared to the control untreated cells.

The morphological examination using DAPI staining also revealed apoptotic cell death of MDMB-231 cells which is characterized by chromatin condensation along with the appearance of numerous fragmented nuclei (Figure 12).

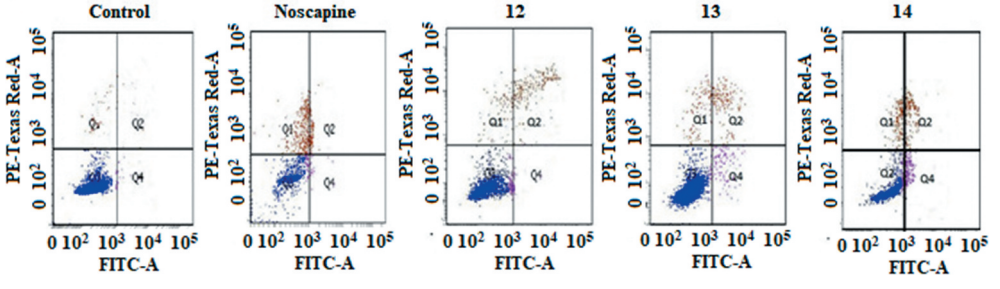

Figure 11. Flow cytometry analysis of phosphatidylserine (PS) exposure in MDAMB-231 cells treated with noscapine and its 9-arylimino noscapinoids, 12–14 with 25 µM for 72 hours and compared with non treated control cells. Annexin-V and propidium iodide (PI) were used to distinguish among three subpopulations of cells: PI- and AnnexinV- cells represent viable cells with intact membrane and preserved amino-phospholipid asymmetry, PI- and Annexin V+ cells represent early apoptotic cells with intact cellular membrane exposing phosphatidylserine, whereas PI+ and Annexin V+ cells represent late apoptotic cells with compromised asymmetry and membrane permeability. Representative results of three independent experiments.

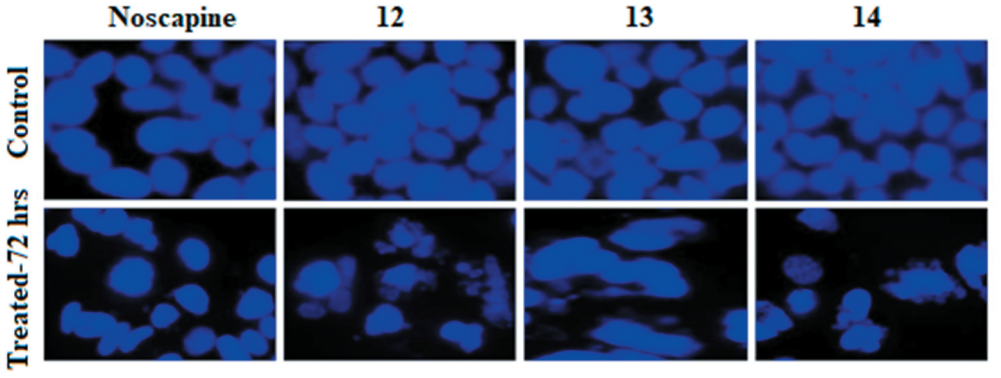

Figure 12. Alteration in morphological features such as chromatin condensation, plasma membrane blebbing, and appearance of apoptotic bodies with treatment of noscapinoids indicate apoptotic cells. Panels show morphological evaluation of nuclei stained with DAPI from control cells (upper panels) and cells treated with 25 μM concentration of noscapine and 9-arylimino noscapinoids, 12–14 (lower panels) for 72 hours using fluorescence microscopy.

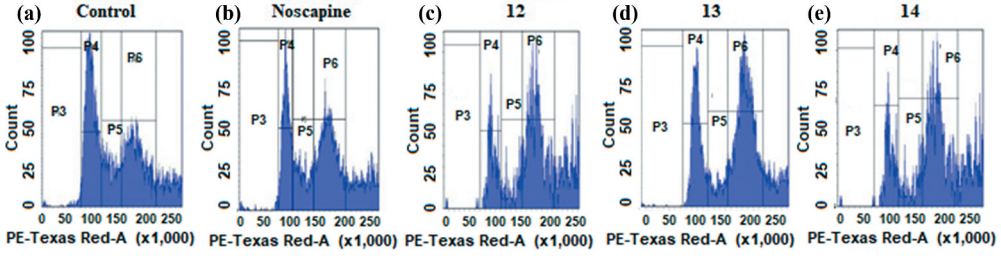

Figure 13. Noscapine and its 9-arylimino derivatives, 12–14 inhibit cell cycle progression at mitosis followed by the appearance of a characteristic hypodiploid (sub-G1) DNA peak, indicative of apoptosis. Panels A-E depict analyses of cell cycle profile, determined by flow cytometry using MDAMB-231 cells treated with 25 μM concentration of noscapine and its derivatives at 72 hours of treatment. The cells of populations P3 are in Sub-G1 phase, P4 are in G1 phase, P5 are in S phase and P6 are in G2/M phase.

9-Arylimino noscapinoids alter cell cycle and mitotic arrest at G_2/M phase

The effect of noscapine and 9-arylimino noscapinoids 12–14 at a concentration of 25 μM on the cell cycle profile of MDAMB-231 was examined based on FACS analysis (Figure 13). The fluorescently labelled DNA accumulation is a good indicator of cell cycle progression and cell death. The unreplicated cells with 2 N DNA represent the G1 phase, while duplicated cells with 4 N DNA represent G2 and M phases. The cells during DNA duplication with peaks between 2 N and 4 N DNA represent S phase. The cells with less than 2 N DNA represent dying cells that degrade their DNA to different extents. The treatment of MDAMB-231 cells with 25 μM of the test compound for 72 h led to significant perturbations of cell cycle profile. The FACS analysis revealed high accumulation of cells in the G2/M phase at 72 h of treatment with noscapine and 9-arylimino noscapinoids 12–14 compared to the untreated cells (Table 6). In contrast to G2/M block, the characteristic hypodiploid DNA content peak (sub-G1) was observed to rise at 72 h of

Table 6. Effect of noscapine and its 9-arylimino noscapinoids, 12–14 on cell cycle progression of MDAMB-231 cells treated with 25 μM solution for 72 hours before being stained with propidium iodide for cell cycle analysis.

	72 hours			
	Sub-G_1	*G_0/G_1*	*S*	*G_2/M*
Control	1.5	13.3	14.4	9.2
Noscapine	4.3	18.1	10.3	15.3
12	7.3	15.4	11.7	22.4
13	11.7	16.3	10.6	25.9
14	13.7	20.2	13.6	31.1

treatment. The progressive generation of cells having hypodiploid DNA content reflects the existence of fragmented DNA, indicating dying cells.

Conclusion

We have strategically designed 9-arylimino noscapinoids of natural lead molecule, noscapine in quest of accelerating its anticancer activity. We have also provided the simplest methods for the direct and regioselective modification of noscapine scaffold to produce the 9-arylimino derivatives in high yields. All the three molecules, 12–14 developed have shown increased antiproliferative activity to cancer cells based on our extensive cellular study using two human breast cancer cell lines (MCF-7 and MDAMB-231) and a panel of primary breast tumour cells. Therefore, these novel molecules may prove efficacious not only in the treatment of breast carcinoma, but also for other type of cancers. Our results compel us to continue to examine the effects of these novel molecules on in vivo animal experiment with the final goal of taking it to the human clinical study.

Acknowledgements

We would like to acknowledge OHEPEE, Govt. of Odisha for providing financial support through World Bank under Centre of Excellence in Natural Products and Therapeutics, Sambalpur University. We are grateful to Dr Manu Lopus and UM-DAE Centre for Excellence in Basic Sciences, Mumbai for providing extended facilities. We are also grateful to Satyandra Kumar Singh, Center for Advance Research, Stem Cell and Tissue Culture Laboratory, King George's Medical University for providing extended facilities to test the molecules with primary breast tumour cells.

Disclosure statement

No potential conflict of interest was reported by the authors.

Funding

This work was supported by the OHEPEE Govt. of Odisha [OHEPEE-SU].

References

[1] M.A. Jordan and L. Wilson, *Microtubules as a target for anticancer drugs*, Nat. Rev. Cancer 4 (2004), pp. 253–265. doi:10.1038/nrc1317.

[2] E.K. Rowinsky, *The development and clinical utility of the taxane class of antimicrotubule chemotherapy agents*, Annu. Rev. Med. 48 (1997), pp. 353–374. doi:10.1146/annurev.med.48.1.353.

[3] J. Crown and M. O'Leary, *The taxanes: An update*, Lancet 355 (2000), pp. 1176–1178. doi:10.1016/S0140-6736(00)02074-2.

[4] C. Theiss and K. Meller, *Taxol impairs anterograde axonal transport of microinjected horseradish peroxidase in dorsal root ganglia neurons in vitro*, Cell Tissue Res. 299 (2000), pp. 213–224. doi:10.1007/s004419900120.

[5] K.S. Topp, K.D. Tanner, and J.D. Levine, *Damage to the cytoskeleton of large diameter sensory neurons and myelinated axons in vincristine-induced painful peripheral neuropathy in the rat*, J. Comp. Neurol. 424 (2000), pp. 563–576. doi:10.1002/1096-9861(20000904)424:43.0.CO:2-U.

[6] K. Ye, Y. Ke, N. Keshava, J. Shanks, J.A. Kapp, R.R. Tekmal, J. Petros, and H.C. Joshi, *Opium alkaloid noscapine is an antitumor agent that arrests metaphase and induces apoptosis in dividing cells*, Proc. Natl. Acad. Sci. U.S.A. 95 (1998), pp. 1601–1606. doi:10.1073/pnas.95.4.1601.

[7] B. Dahlström, T. Mellstrand, C.G. Löfdahl, and M. Johansson, *Pharmacokinetic properties of noscapine*, Euro. J. Clin. Pharma. 22 (1982), pp. 535–539. doi:10.1007/BF00609627.

[8] M.O. Karlsson, B. Dahlstrom, S.A. Eckernas, M. Johansson, and A.T. Alm, *Pharmacokinetics of oral noscapine*, Eur. J. Clin. Pharmacol. 39 (1990), pp. 275–279. doi:10.1007/BF00315110.

[9] L.N. Jensen, L.L. Christrup, L. Jacobsen, J. Bonde, and H. Bundgaard, *Relative bioavailability in man of noscapine administered in lozenges and mixture*, Acta Pharm. Nord. 4 (1992), pp. 309–312.

[10] Y. Ke, K. Ye, H.E. Grossniklaus, D.R. Archer, H.C. Joshi, and J.A. Kapp, *Noscapine inhibits tumor growth with little toxicity to normal tissues or inhibition of immune responses*, Can. Immunol. Immunother. 49 (2000), pp. 217–225. doi:10.1007/s002620000109.

[11] J. Zhou, K. Gupta, S. Aggarwal, R. Aneja, R. Chandra, D. Panda, and H.C. Joshi, *Brominated derivatives of noscapine are potent microtubule-interfering agents that perturb mitosis and inhibit cell proliferation*, Mol. Pharma. 63 (2003), pp. 799–807. doi:10.1124/mol.63.4.799.

[12] J.W. Landen, R. Lang, S.J. McMahon, N.M. Rusan, A.M. Yvon, A.W. Adams, M.D. Sorcinelli, R. Campbell, P. Bonaccorsi, J.C. Ansel, D.R. Archer, P. Wadsworth, C.A. Armstrong, and H. C. Joshi, *Noscapine alters microtubule dynamics in living cells and inhibits the progression of melanoma*, Can. Res. 62 (2002), pp. 4109–4114.

[13] J. Zhou, K. Gupta, J. Yao, K. Ye, D. Panda, P. Giannakakou, and H.C. Joshi, *Paclitaxel-resistant human ovarian cancer cells undergo c-Jun NH2-terminal kinase-mediated apoptosis in response to noscapine*, J. Biol. Chem. 277 (2002), pp. 39777–39785. doi:10.1074/jbc.M203927200.

[14] N.K. Manchukonda, B. Sridhar, P.K. Naik, H.C. Joshi, and S. Kantevari, *Copper (I) mediated facile synthesis of potent tubulin polymerization inhibitor, 9-amino-α-noscapine from natural α-noscapine*, Bio. Med. Chem. Lett. 22 (2012), pp. 2983–2987. doi:10.1016/j.bmcl.2012.02.033.

[15] N.K. Manchukonda, P.K. Naik, S. Santoshi, M. Lopus, S. Joseph, and S. Kantevari, *Rational design, synthesis, and biological evaluation of third generation α-noscapine analogues as potent tubulin binding anti-cancer agents*, PloS One 8 (2013), pp. e77970. doi:10.1371/journal.pone.0077970.

[16] S. Santoshi, P.K. Naik, and H.C. Joshi, *Rational design of novel anti-microtubule agent (9-azido-noscapine) from quantitative structure activity relationship (QSAR) evaluation of noscapinoids*, J. Biomol. Scr. 16 (2011), pp. 1047–1058. doi:10.1177/1087057111418654.

[17] M.A. Oliva, A.E. Prota, J. Rodríguez-Salarichs, Y.L. Bennani, J. Jiménez-Barbero, K. Bargsten, Á. Canales, M.O. Steinmetz, and J.F. Díaz, *Structural basis of noscapine activation for tubulin binding*, J. Med. Chem. 63 (2020), pp. 8495–8501. doi:10.1021/acs.jmedchem.0c00855.

[18] H.J. Berendsen, D. van der Spoel, and R. van Drunen, *GROMACS: A message-passing parallel molecular dynamics implementation*, Comp. Phys. Comm. 91 (1995), pp. 43–56. doi:10.1016/0010-4655(95)00042-E.

[19] S. Santoshi and P.K. Naik, *Molecular insight of isotypes specific β-tubulin interaction of tubulin heterodimer with noscapinoids*, J. Comp-Aid. Mol. Des. 28 (2014), pp. 751–763. doi:10.1007/s10822-014-9756-9.

[20] I. Ali, A. Haque, K. Saleem, and M.F. Hsieh, *Curcumin-I Knoevenagel's condensates and their Schiff's bases as anticancer agents: Synthesis, pharmacological and simulation studies*, Bio-Org. Med. Chem. 21 (2013), pp. 3808–3820. doi:10.1016/j.bmc.2013.04.018.

[21] S.M. Sondhi, S. Arya, R. Rani, N. Kumar, and P. Roy, *Synthesis, anti-inflammatory and anticancer activity evaluation of some mono-and bis-Schiff's bases*, Med Chem Res. 21 (2012), pp. 3620–3628. doi:10.1007/s00044-011-9899-3.

[22] S. Santoshi, N.K. Manchukonda, C. Suri, M. Sharma, B. Sridhar, S. Joseph, M. Lopus, S. Kantevari, I. Baitharu, and P.K. Naik, *Rational design of biaryl pharmacophore inserted noscapine derivatives as potent tubulin binding anticancer agents*, J. Comp-Aid. Mol. Des. 29 (2015), pp. 249–270. doi:10.1007/s10822-014-9820-5.

[23] P.K. Naik, B.P. Chatterji, S.N. Vangapandu, R. Aneja, R. Chandra, S. Kanteveri, and H.C. Joshi, *Rational design, synthesis and biological evaluations of amino-noscapine: A high affinity tubulin-binding noscapinoid*, J. Comp-Aid. Mol. Des. 25 (2011), pp. 443–454. doi:10.1016/j.jmgm.2011.03.004.

[24] R. Aneja, S.N. Vangapandu, M. Lopus, R. Cha.ndra, D. Panda, and H.C. Joshi, *Development of a novel nitro-derivative of noscapine for the potential treatment of drug-resistant ovarian cancer and T-cell lymphoma*, Mol. Pharm. 69 (2006), pp. 1801–1809. doi:10.1124/mol.105.021899.

[25] R.A. Friesner, J.L. Banks, R.B. Murphy, T.A. Halgren, J.J. Klicic, D.T. Mainz, M.P. Repasky, E. H. Knoll, M. Shelley, J.K. Perry, D.E. Shaw, P. Francis, and P.S. Shenkin, *Glide: A new approach for rapid, accurate docking and scoring. 1. Method and assessment of docking accuracy*, J. Med. Chem. 47 (2004), pp. 1739–1749. doi:10.1021/jm0306430.

[26] T.A. Halgren, R.B. Murphy, R.A. Friesner, H.S. Beard, L.L. Frye, W.T. Pollard, and J.L. Banks, *Glide: A new approach for rapid, accurate docking and scoring. 2. Enrichment factors in database screening*, J. Med. Chem. 47 (2004), pp. 1750–1759. doi:10.1021/jm030644s.

[27] R. Zhou, R.A. Friesner, A. Ghosh, R.C. Rizzo, W.L. Jorgensen, and R.M. Levy, *New linear interaction method for binding affinity calculations using a continuum solvent model*, J. Phys. Chem. 105 (2001), pp. 10388–10397. doi:10.1021/jp011480z.

[28] D.A. Case, R.M. Betz, D.S. Cerutti, T.E. Cheatham III, T.A. Darden, R.E. Duke, T.J. Giese, H. Gohlke, A.W. Goetz, N. Homeyer, S. Izadi, P. Janowski, J. Kaus, A. Kovalenko, T.S. Lee, S. LeGrand, P. Li, C. Lin, T. Luchko, R. Luo, B. Madej, D. Mermelstein, K.M. Merz, G. Monard, H. Nguyen, H. T. Nguyen, I. Omelyan, A. Onufriev, D.R. Roe, A. Roitberg, C. Sagui, C.L. Simmerling, W. Botello-Smith, J. Swails, R.C. Walker, J. Wang, R.M. Wolf, X. Wu, L. Xiao, and P.A. Kollman, *Amber 2016*, Univ. Cal. San Franc, 2016.

[29] J. Wang, W. Wang, P.A. Kollman, and D.A. Case, *Automatic atom type and bond type perception in molecular mechanical calculations*, J. Mol. Graph. Model. 25 (2006), pp. 247–260. doi:10.1016/j.jmgm.2005.12.005.

[30] A. Jakalian, D.B. Jack, and C.I. Bayly, *Fast, efficient generation of high quality atomic charges. AM1-BCC model: II. Parameterization and validation*, J. Comp. Chem. 23 (2002), pp. 1623–1641. doi:10.1002/jcc.10128.

[31] W.L. Jorgensen, J. Chandrasekhar, J.D. Madura, R.W. Impey, and M.L. Klein, *Comparison of simple potential functions for simulating liquid water*, J. Chem. Phys. 79 (1983), pp. 926–935. doi:10.1063/1.445869.

[32] J.P. Ryckaert, G. Ciccotti, and H.J. Berendsen, *Numerical integration of the cartesian equations of motion of a system with constraints: Molecular dynamics of n- alkanes*, J. Comp. Phys. 23 (1977), pp. 327–341. doi:10.1016/0021-9991(77)90098-5.

[33] T. Darden, D. York, and L. Pedersen, *Particle mesh Ewald: An N. log (N) method for Ewald sums in large systems*, J. Chem. Phys. 98 (1993), pp. 10089–10092. doi:10.1063/1.464397.

[34] U. Essmann, L. Perera, M.L. Berkowitz, T. Darden, H. Lee, and L.G. Pedersen, *A smooth particle mesh Ewald method*, J. Chem. Phys. 103 (1995), pp. 8577–8593. doi:10.1063/1.470117.

[35] P.A. Kollman, I. Massova, C. Reyes, B. Kuhn, S. Huo, L. Chong, M. Lee, T. Lee, Y. Duan, and W. Wang, *Calculating structures and free energies of complex molecules: Combining molecular*

mechanics and continuum models, Acc. Chem. Res. 33 (2000), pp. 889–897. doi:10.1021/ar000033j.

[36] E. Hamel and C.M. Lin, *Glutamate-induced polymerization of tubulin: Characteristics of the reaction and application to the large scale purification of tubulin*, Arch. Biochem. Biophys. 209 (1981), pp. 29–40. doi:10.1016/0003-9861(81)90253-8.

[37] D. Panda, G. Chakrabarti, J. Hudson, K. Pigg, H.P. Miller, L. Wilson, and R.H. Himes, *Suppression of microtubule dynamic instability and treadmilling by deuterium oxide*, J. Biochem. 39 (2000), pp. 5075–5081. doi:10.1021/bi992217f.

[38] M.M. Bradford, *A rapid and sensitive method for the quantitation of microgram quantities of protein utilizing the principle of protein-dye binding*, Anal. Biochem. 72 (1976), pp. 248–254. doi:10.1016/0003-2697(76)90527-3.

[39] P.K. Naik, M. Lopus, R. Aneja, S.N. Vangapandu, and H.C. Joshi, *In silico inspired design and synthesis of a novel tubulin-binding anti-cancer drug: Folate conjugated noscapine (Targetin)*, J. Comp-Aid. Mol. Des. 26 (2012), pp. 233–247. doi:10.1007/s10822-011-9508-z.

[40] R. Aneja, S.N. Vangapandu, M. Lopus, V.G. Viswesarappa, N. Dhiman, A. Verma, R. Chandra, D. Panda, and H.C. Joshi, *Synthesis of microtubule-interfering halogenated noscapine analogs that perturb mitosis in cancer cells followed by cell death*, Biochem. Pharm. 72 (2006b), pp. 415–426. doi:10.1016/j.bcp.2006.05.004.

[41] N. Jain, D. Yada, T.B. Shaik, G. Vasantha, P.S. Reddy, S.V. Kalivendi, and B. Sreedhar, *Synthesis and antitumor evaluation of nitrovinyl biphenyls: Anticancer agents based on allocolchicines*, Chem. Med. Chem. 6 (2011), pp. 859–868. doi:10.1002/cmdc.201100019.